

Journal of Biomedical Optics

BiomedicalOptics.SPIEDigitalLibrary.org

Aptamer-based fiber sensor for thrombin detection

Luís Coelho

José Manuel Marques Martins de Almeida

José Luís Santos

Pedro Alberto da Silva Jorge

Maria Cristina L. Martins

Diana Viegas

Raquel B. Queirós

SPIE.

Luís Coelho, José Manuel Marques Martins de Almeida, José Luís Santos, Pedro Alberto da Silva Jorge, Maria Cristina L. Martins, Diana Viegas, Raquel B. Queirós, "Aptamer-based fiber sensor for thrombin detection," *J. Biomed. Opt.* **21**(8), 087005 (2016), doi: 10.1117/1.JBO.21.8.087005.

Aptamer-based fiber sensor for thrombin detection

Luíś Coelho,^{a,*} José Manuel Marques Martins de Almeida,^{a,b} José Luís Santos,^a Pedro Alberto da Silva Jorge,^a Maria Cristina L. Martins,^{c,d,e} Diana Viegas,^d and Raquel B. Queirós^f

^aUniversity of Porto, CAP/INESC TEC—Technology and Science and FCUP—Faculty of Sciences, Rua do Campo Alegre, 4150-179 Porto, Portugal

^bUniversidade de Trás-os-Montes e Alto Douro, Department of Physics, School of Sciences and Technology, Apartado 1013, 5001-801 Vila Real, Portugal

^cUniversidade do Porto, i3S—Instituto de Investigação e Inovação em Saúde, Portugal

^dUniversidade do Porto, INEB—Instituto de Engenharia Biomédica, Rua Alfredo Allen, 208, 4200-135 Porto, Portugal

^eUniversidade do Porto, ICBAS—Instituto de Ciências Biomédicas Abel Salazar, Rua de Jorge Viterbo Ferreira 228, 4050-313 Porto, Portugal

^fINL—International Iberian Nanotechnology, Avenida Mestre José Veiga s/n, 4715-330 Braga, Portugal

Abstract. The detection of thrombin based on aptamer binding is studied using two different optical fiber-based configurations: long period gratings coated with a thin layer of titanium dioxide and surface plasmon resonance devices in optical fibers coated with a multilayer of gold and titanium dioxide. These structures are functionalized and the performance to detect thrombin in the range 10 to 100 nM is compared in transmission mode. The sensitivity to the surrounding refractive index (RI) of the plasmonic device is higher than 3100 nm RIU⁻¹ in the RI range 1.335 to 1.355, a factor of 20 greater than the sensitivity of the coated grating. The detection of 10 nM of thrombin was accomplished with a wavelength shift of 3.5 nm and a resolution of 0.54 nM. ©2016 Society of Photo-Optical Instrumentation Engineers (SPIE) [DOI: 10.1117/1.JBO.21.8.087005]

Keywords: surface plasmon resonance; long period fiber gratings; titanium dioxide; fiber optic refractometer; thrombin-binding aptamer.

Paper 160046RR received Jan. 23, 2016; accepted for publication Aug. 1, 2016; published online Aug. 18, 2016.

1 Introduction

Low cost analysis systems capable of providing measurements of analyte in a short-time period or even in real time at low concentration are paramount in many fields, such as medicine, drugs detection, or food safety. Fiber optic devices applied to biosensing are an appealing solution that can fulfill these requirements. It is important to recognize the advantages of these biosensors including their compatibility to a wide range of surface modifications, chemical-inertness, their compactness and cost effectiveness, and their potential for remote sensing.¹

Thrombin is a key protein playing an important role in the blood coagulation cascade and in homeostasis.^{2,3} The concentration of thrombin in blood is quite variable and several clotting factors are affected by thrombin concentrations.⁴ The use of aptamer-based assays for detection and quantification of thrombin has several advantages due to their high specificity and affinity to its targets, considering their ability to fold into numerous tertiary conformations.^{5,6} Moreover, aptamers can be generated and synthesized in a large quantity *in vitro* in a very reproducible way.^{7,8} They are thermally and chemically very stable, increasing their use in time without losing its ability to bind specifically to their target.^{9,10}

The detection of thrombin could be achieved through the manipulation of a specific thrombin-binding aptamer (TBA) that inhibits the activity of thrombin.¹¹ This capability of regulating thrombin activity using synthetic compounds is a major mark in prevention of thrombosis.

The immobilization of the DNA on a waveguide surface leads to changes in the spectral response, which can be measurable with specific optical fiber components, such as long

period fiber grating (LPFG) or surface plasmon resonance (SPR) structures. Typical LPFG and SPR fiber-based sensors show great potential to be used as biosensing devices coupled with the well-known advantages of optical fiber sensors.^{12–14}

LPFG relies on coupling light from the core mode of a single-mode fiber (SMF) into cladding modes through the introduction of a periodic modulation in the refractive index (RI) of the fiber core.¹⁵ The period of the RI modulation is such that a phase matching condition between the core mode and a forward propagating cladding mode of an optical fiber occurs at a given wavelength:¹⁶

$$\lambda = [n_{\text{eff}}(\lambda) - n_{\text{clad}}^i(\lambda)]\Lambda, \quad (1)$$

where $n_{\text{eff}}(\lambda)$ is the effective RI of the core mode at wavelength λ , $n_{\text{clad}}^i(\lambda)$ is the effective RI of the i 'th cladding mode, and Λ is the period of the LPFG. Several attenuation bands are formed in the transmission spectrum of the fiber.¹⁷

An evanescent field reaches outside the cladding perimeter, thus making LPFGs sensitive to the optical properties of materials surrounding the fiber. This characteristic has led to studies of LPFGs coated with a number of materials which are chosen to change their optical properties in response to an external stimulation.¹⁸

Optical fiber sensors based on SPR, on the other hand, have been studied using different configurations and applied to different geometries.¹⁹ SPR can be defined as a charge-density oscillation that, in certain conditions, can be generated at the interface of two media, a metal and a dielectric, with dielectric constants of opposite signs. The charge density oscillation is associated with an electromagnetic wave with the evanescent

*Address all correspondence to: Luíś Coelho, E-mail: lccoelho@gmail.com

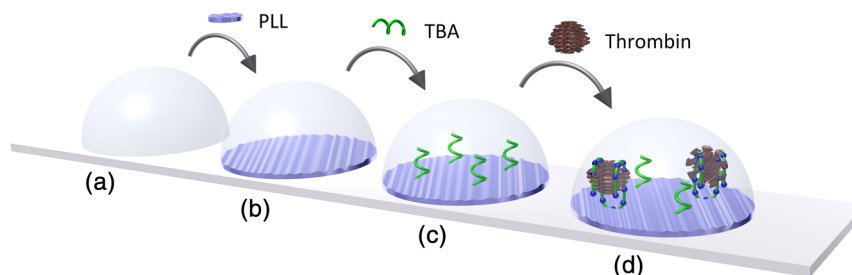


Fig. 1 Detailed scheme of the biosensor binding principle: (a) clean surface, (b) surface functionalized with PLL, (c) incubated with TBA, and (d) in the presence of thrombin.

field at the interface decaying exponentially into both media.²⁰ The result is an attenuation band in the transmission spectra whose wavelength position is highly dependent on the external RI.

In this work, two different types of refractometric platforms using optical fibers devices, LPFGs and SPRs, were validated to be used as biosensing devices, for the detection of thrombin using a 15-mer single-stranded DNA aptamer-based probe as a model system for protein detection.

2 Materials and Methods

2.1 Reagents and Solutions

The thrombin oligonucleotide sequence (5'-amine-GGTTGGTGTGGTTGG-3') with a synthesis scale of 0.2 μ M, purification HPLC, and 5' amine modification was purchased from Sigma-Aldrich (Spain). Human- α -thrombin was obtained from Haematologic Technologies in a concentration of 1 mg mL⁻¹ (50 mM sodium phosphate, 150 mM sodium chloride, pH 6.5, 3757 U mg⁻¹). The solutions of thrombin used in each assay were prepared by dilution in 10 mM of phosphate-buffered saline from Sigma-Aldrich (Spain) in Eppendorf's blocked with 1% bovine serum albumin, from Merck, aliquoted and stored at -80°C. Salts for buffer solutions were prepared in ultra-pure water, <15 M Ω cm at 25°C. Hydrochloric acid (HCl), isopropanol (IPA), sodium hypochlorite, ethanol, and magnesium chloride were purchased from Panreac (Spain), tris (hydroxymethyl)aminomethane (Tris), 0.1 % (w/v) poly-L-lysine (PLL), potassium chloride (KCl), sodium chloride (NaCl), SSPE buffer 20 \times concentrate [1 \times = 0.150 M sodium chloride, 0.010 M sodium phosphate, 0.001 M ethylenediaminetetraacetic acid (EDTA)] and Tris-EDTA (TE) were obtained from Sigma (Germany). The buffers used in this work were aptamer resuspension buffer: TE (10 mM Tris pH 7.5 to 8.0; 1 mM EDTA); aptamer immobilization buffer: SSPE (1:10), (diluted from 20 \times SSPE); affinity buffer (50 mM Tris-HCl pH 7.4, 250 mM NaCl, 5 mM MgCl₂) and measurement buffer (10 mM Tris-HCl pH 7.4, 100 mM KCl). All the reagents were of analytical grade.

2.2 Optical Fiber Sensors Fabrication

Both sensing structures were produced from the regular SMF28 from Corning, Inc., following a specific protocol. The LPFG sensors were produced by the electric-arc technique, as described by Rego et al.,²¹ which consists of applying point-by-point short time discharges to the uncoated fiber. The period of the gratings was 396 μ m, a value chosen to produce a resonance wavelength at 1550 nm matching the antisymmetric sixth order cladding mode (LP₁₆) according to Ivanov and Rego.²²

The grating attenuation band value was reached with a sensor length of 45 \pm 5 mm.

The sensitivity to the external medium of the LPFG was enhanced by coating the surface with a 30-nm thin layer of titanium dioxide (TiO₂), the details of the manufacturing process were presented recently.²³ This procedure causes a reduction in the amplitude of the attenuation band. For temperature compensation, the LPFG is coupled to a fiber Bragg grating (FBG) written in hydrogen loaded SMF28 fiber using the phase mask technique with a reflection wavelength peak at 1537.5 nm at room temperature.²⁴

The SPR sensing device was produced using the procedure previously described.²⁵ Briefly, the plastic protective jacket was removed and a 10 mm long section of the fiber was chemically etched by immersion in an aqueous solution with 10 mL of 48% HF during 48 min at 22 C and 60% of humidity until the etched region became \sim 16 μ m in diameter. The sensing region is located at the thinner section, where the evanescent field is able to excite the plasmonic wave. First, the etched region was coated with 2 nm of pure chromium (Cr) to improve the adhesion of gold (Au). Then a 16-nm thick film of Au was deposited around the fiber, followed by a 100-nm thick dielectric layer of TiO₂. The thickness of both metal and dielectric layers was calculated in a previous publication²⁵ to obtain a resonance in the C-band by using the transfer matrix formalism approximation for a SLAB multilayer system.

The metal/dielectric coatings were produced around the cylindrical fiber shape by thermal evaporation of pure titanium (Ti) in a controlled oxygen atmosphere using an electron beam evaporator (Auto 306, Edwards Ltd., United Kingdom) fitted with a rotary system, which improves the homogeneity of the coating.

2.3 Biosensing Principle

Both sensing surfaces were functionalized with PLL, followed by the immobilization of the DNA probe—TBA, for the specific recognition of thrombin. It is well-studied, 15-mer single-stranded DNA that shows good affinity and specificity against thrombin as has been described by Bock et al.²⁶ and does not interact with other plasma proteins or thrombin analogues, such as gamma-thrombin.²⁷

The detailed biosensor principle is illustrated in Fig. 1. First, in Fig. 1(a), the sensing surface was cleaned with IPA and then rinsed with ultra-pure water and dried with nitrogen (N₂). Then in Fig. 1(b), the surface was functionalized with PLL (60 min at room temperature). The polycationic nature of the PLL leads to its electrostatic attraction onto the fiber's negatively charged surface, in an aqueous environment at neutral pH (7.4). After that in Fig. 1(c), the 5'-amine modified TBA (500 nM) was incubated

for 60 min at room temperature for its covalent attachment to the PLL backbone. In the absence of thrombin, the TBA remains at its secondary conformation. In the presence of thrombin, the TBA folds around the protein and forms a TBA/thrombin complex, acquiring the G-quarter (tertiary) conformation [Fig. 1(d)]. The formation of this complex causes an increase in the effective RI, which changes the optical properties of the guided light.

The sensing devices were incubated with several concentrations of thrombin in the affinity buffer for 1 h. The sensor response was measured in the concentration range from 10 to 100 nM. Between all concentrations steps, the sensing device surfaces were washed with Tris-HCl buffer and the transmission spectra were recorded with the optical spectrum analyzer (OSA) in the measurement buffer. After a complete assay, the sensing probe was washed with 5% hypochlorite solution for 30 min, to regenerate the fiber sensor surface for reuse.

2.4 Fiber-Optic Sensing Setup Assembly

The optical characterization entails the setup shown in Fig. 2 with an OSA or equivalent. The characterization setup for the LPFG [Fig. 2(a)] includes a FS2200 Braggmeter (FiberSensing, SA, Portugal), a fluidic system containing a reaction chamber with capacity of 750 μL , and a laptop (not shown) with LabVIEW software that receives and processes the readout information. The LPFG and FBG sensing elements were characterized using the Braggmeter (working in the 1500 to 1600 nm range with 2.5 pm of resolution) and modified to measure signals both in reflection and in transmission modes.

The setup in Fig. 2(b) for the SPR sensing characterization includes a super luminescent diode source (SLD) model S5FC1550S-A2 (Benchtop SLD—Thorlabs, Germany), a fluidic system where the fiber is fixed, and an OSA (ANDO, model AQ 6315B).

Although the Braggmeter is, by design, capable of simultaneously monitoring two sets of sensors, the SPR sensor at low RI values operates outside its spectral window (1500 to 1600 nm). Therefore, the interrogation of the sensors was done using the OSA and SLD for SPR and the FS2200 SA Braggmeter (for the LPFG). The different setups were used together in order to enable the simultaneous measurements and comparison of the sensor devices.

3 Results and Discussion

3.1 Refractive Index Characterization

Both sensing devices were characterized in terms of the surrounding refractive index (SRI) changes. Solutions with different RI values were prepared by adding ethylene glycol to ultrapure water. Thus, solutions with RI from 1.335 to 1.430 can be obtained varying concentrations of the mixture.²⁸ In order to accomplish homogeneous solutions, a magnetic stirrer was used and the measurements were accomplished within 5 min after each mixing.

In parallel to the optical characterization of the fiber sensing devices, the RI of the sample solutions was measured at room temperature ($26 \pm 1^\circ\text{C}$) using an Abbe refractometer (A. Kruss, Optronic, Germany) with an RI resolution of 2.5×10^{-4} .

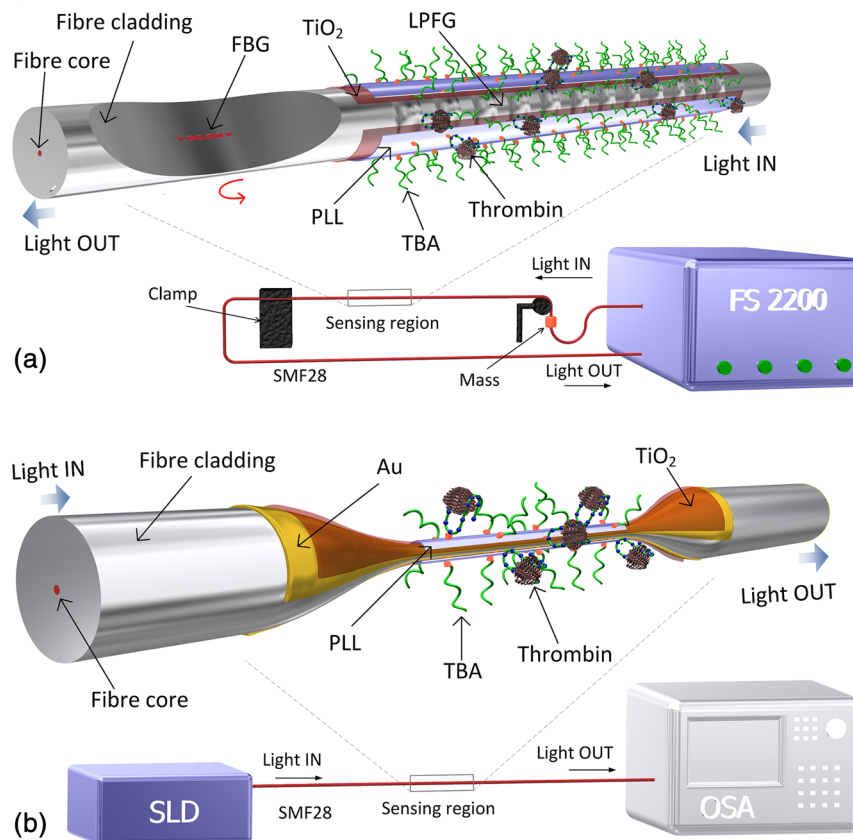


Fig. 2 Scheme of the sensing configurations: (a) long period grating coated with 30 nm of TiO_2 and (b) surface plasmon resonance device in etched single-mode fiber coated with Au and TiO_2 .

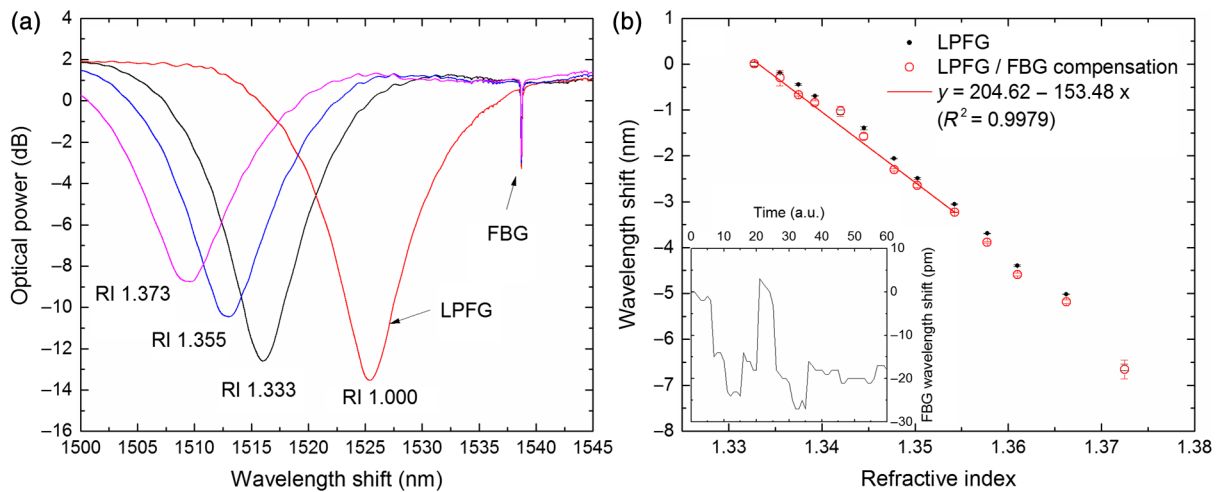


Fig. 3 (a) Spectra of the LPFG for different SRI values, the FBG located at higher wavelength and (b) LPFG wavelength shift to SRI between 1.335 and 1.375 with thermal compensation and with a linear behavior up to 1.355. Inset is the FBG spectral response due to thermal variations.

Solutions with RI in the range from 1.335 to 1.373 were attained.

After each measurement, the sensing device was flushed with 20 ml of IPA and dried with filtered air to avoid contamination to the next sample. Then the spectrum of each sensor was monitored to ensure that the initial spectral conditions were verified.

The characterization of the sensors enables the calculation of the sensor sensitivity through the changes of the spectrum due to changes of the effective SRI.

The wavelength dependence with the external RI of the LPFG and the SPR is presented in Figs. 3 and 4, respectively. The resonance peak of these kind of devices is, in most cases, asymmetric, however, the lower part of the attenuation bands can be fitted by a symmetric curve with reasonable accuracy. To perform this analysis, the minimum optical power of the band was evaluated and then considering only the points 30% above this minimum, a Gaussian function was fitted and all the parameters were extracted, such as the wavelength position and the minimum optical power.

In both sensing devices, the dependence of the wavelength with the RI is nonlinear, nevertheless, a rough linear fitting can be made in the RI range from 1.335 to 1.355 where the

corresponding changes induced by the thrombin detection are expected.

Figure 3(a) shows the spectra of the LPFG when placed in different RI solutions. By monitoring the position of the resonant peak as a function of the SRI, it is possible to estimate the spectral sensitivity of the sensor, obtaining the traces presented in Fig. 3(b). Even though the LPFGs are sensitive to temperature, when coupled to the FBG, which is insensitive to the SRI, these variations can be compensated.²⁹ The inset of Fig. 3(b) presents the wavelength shift of the FBG transmission peak showing the thermal variation of each measuring point, which is used to calibrate the LPFG data points leading to a sensitivity to the SRI of $153.5 \text{ nm RIU}^{-1}$, which is higher than a bare LPFG in the same RI range, as reported in a previous publication.³⁰

In Fig. 4(a), the spectra obtained with the SPR at different SRI values are presented. Although the shape of the attenuation band is wider, the wavelength shift attained for the same RI samples is more than 20 times higher compared to the LPFG. The data points corresponding to the SPR sensor presented in Fig. 4(b) follow an exponential behavior. However, in the expected working RI range, from 1.335 to 1.355, a linear fit leads to a calculated sensitivity higher than 3000 nm RIU^{-1} .

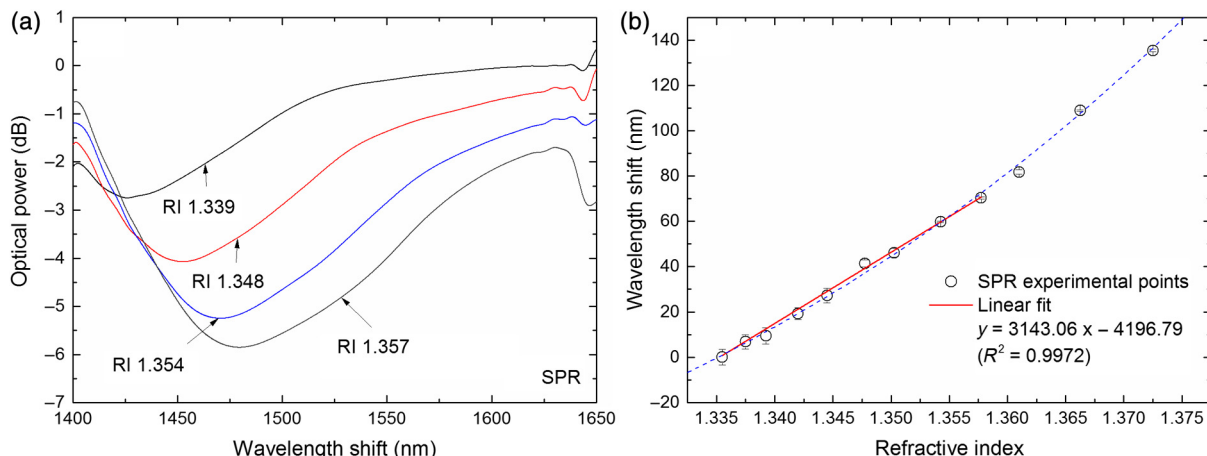


Fig. 4 (a) Spectra of the SPR at different SRI liquid samples and (b) SPR wavelength shift to different SRI samples with a linear fit in the RI range from 1.335 to 1.355.

The low temperature variations are not an issue when the SPR device is considered. The effect of temperature using an SPR sensor was discussed previously.²⁵ Despite the material properties of the SPR layers being affected by temperature with thermal expansion, these changes are not reflected in the optical properties when such low variations are considered. In addition, it is known³¹ that the RI of liquids change with temperature by a factor of $\sim 1.73 \times 10^{-4} \text{C}^{-1}$, which can be neglected for this working range.

3.2 Thrombin-Binding Aptamer-Based Optical Fiber Sensing Systems Operation

The sensor performance was tested against varying concentrations of thrombin (10 to 100 nM) in the measuring buffer solution, using both sensing systems, LPFG and SPR-based.

Figure 5(a) displays the spectra of the LPFG coated with 30 nm of TiO_2 in series with an FBG across the functionalization procedure with PLL, the immobilization of the DNA probe, the thrombin detection with a concentration of 100 nM, and the regeneration using hypochlorite.

The LPFG response (wavelength shift) to the surface functionalization and thrombin detection measured in buffer solution are shown in Fig. 5(b). Well-defined steps, corresponding to the different layers attached to the LPFG surface, were attained after the thermal effect correction calculated with the FBG.

The transmitted spectra of the coupled FBG in Fig. 5(c) show small variations of the temperature detected along the functionalization and detection procedure. The correspondent wavelength shift is quantified in Fig. 5(d) and is used for the LPFG calibration considering the intrinsic temperature sensitivities of each structure.

The PLL coating causes a negative wavelength shift of about 128 pm, which reflects an increase of the effective RI (as reported by Westwood et al. in 2013³²). The immobilization of the DNA probe, TBA, causes a resonance peak shift of 165 pm. The binding of TBA-thrombin causes a wavelength shift of about 100 pm. The resolution can be calculated by using the following mathematical equation:

$$R = \frac{\delta C}{\delta \lambda} \sigma, \quad (2)$$

where C is the thrombin concentration, $\delta \lambda$ is the wavelength shift, and σ is the higher standard deviation of the two stages in a certain step. The resolution for this event is about 10.4 nM for a concentration of 100 nM.

It is visible in the regeneration step with hypochlorite that the DNA probe was removed from the sensor leaving the surface completely regenerated and ready for a new functionalization procedure.

The SPR spectra obtained at each step of the thrombin detection are shown in Fig. 6. As previously mentioned, the SPR

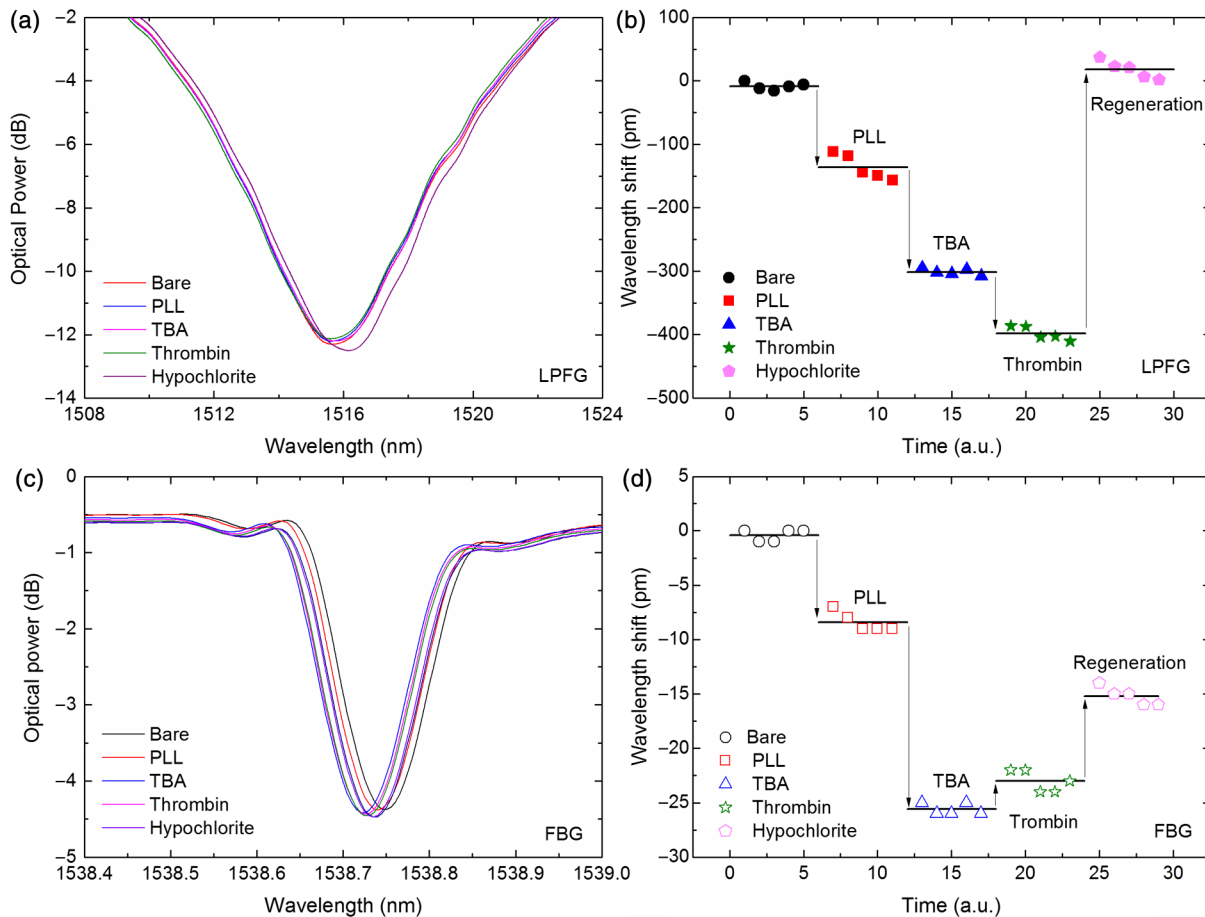


Fig. 5 (a) LFBG spectra after each procedure step (bare, PLL, TBA, thrombin binding, and regeneration), (b) wavelength shift of the LPFG after temperature correction, (c) transmission FBG spectra, and (d) FBG wavelength shift behavior. Measurements were done in Tris-HCl buffer solution at room temperature.

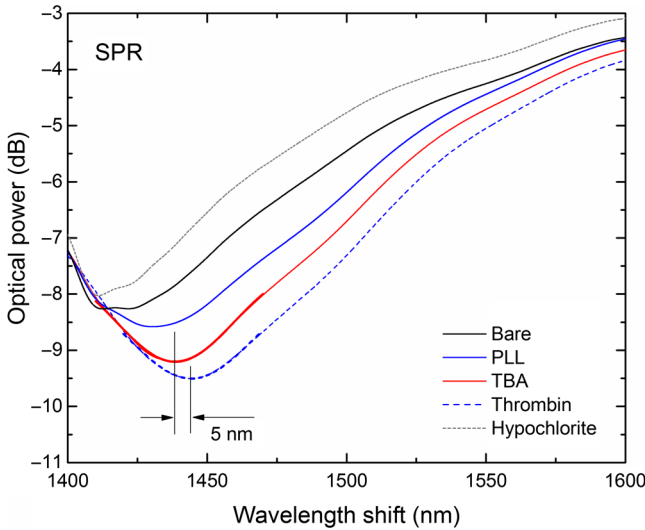


Fig. 6 Average SPR spectra of five measurements at each procedure step with (bare, PLL, TBA, thrombin binding, and regeneration). Measurements were done in Tris-HCl buffer solution at room temperature.

spectrum shape is wider with lower attenuation due to the polarization effect (which is not controlled in this experiment), although with a sensitivity 20 times higher.

The spectral features of the SPR in transmission mode are illustrated in Fig. 7 in terms of the wavelength shift [Fig. 7(a)] and the optical power shift [Fig. 7(b)] of the attenuation band minimum considering the functionalization steps, the thrombin detection, and the regeneration of the sensor. Wavelength shifts of 10.3 and 8.2 nm for the PLL coating and the TBA immobilization, respectively, were achieved. The step corresponding to the thrombin detection shows a variation of 4.94 nm, which is a considerable improvement when compared to ~100 pm from the LPFG results.

The thrombin detection resolutions using the SPR sensor for the wavelength and intensity modulations were calculated as 1.08 and 0.13 nM, respectively.

3.3 Sensor Performance to Thrombin Detection

The analytical performance of TBA-based optical fiber sensing systems was investigated by using target thrombin with different concentrations (10, 50, and 100 nM).

The results of the wavelength shift when applying different concentrations of thrombin normalized to the TBA are shown in Fig. 8. The SPR results are represented with empty symbols while the LPFG are represented by the filled ones.

In the SPR configuration, a resonance shift of ~3.5 nm is observed for 10 nM of thrombin. From this data, and considering the system signal-to-noise-ratio, a resolution of 0.54 nM can be calculated. Increasing the concentration to 50 nM leads to a new shift of the resonance of about 1.5 nm, corresponding to a total accumulated shift of 5 nm after the TBA immobilization. A new increase of the concentration to 100 nM results in practically no observable shift. The sensor displays a similar

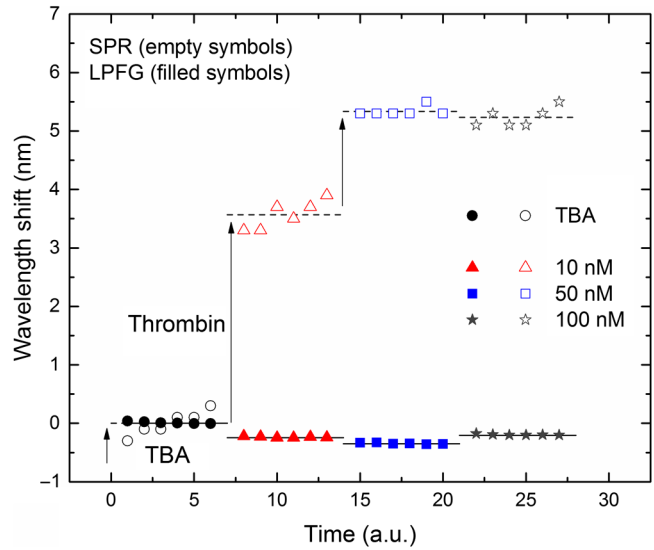


Fig. 8 Wavelength shift of the LPFG (filled symbols) and the SPR (empty symbols) in Tris buffer measurement solution after the TBA immobilization and after thrombin incubation at 10, 50, and 100 nM.

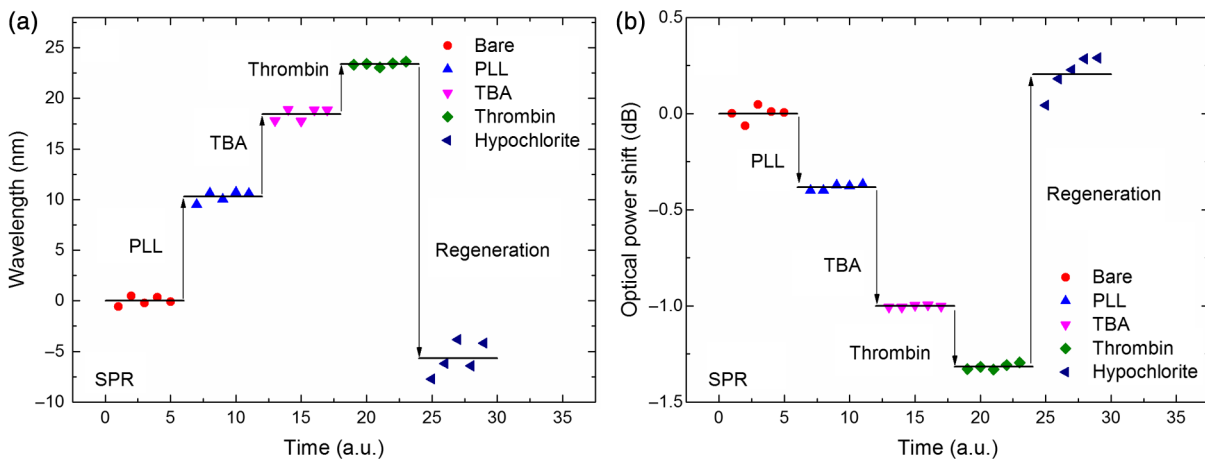


Fig. 7 Results of the (a) SPR wavelength and (b) optical power shifts after each procedure step (PLL, TBA, thrombin, and hypochlorite). Measurements were done in Tris-HCl buffer solution at room temperature. The optical power shift follows the same behavior with well-defined steps allowing the sensor to be used in intensity modulation mode. In both modes, the functionalization layers are completely removed from the surface during the regeneration step enabling new measurement cycles.

Table 1 Comparison of the results herein presented with other researchers' works considering different parameters.

References	Allsop et al. ¹⁴	Lin et al. ³⁵	Park et al. ³⁶	Razquin et al. ³⁷	This work
Detection method	Optical SPR	Optical	Spectroscopic/electrochemical	Optical LMR	Optical SPR/LPFG
Time for analysis	20 min	80 min	20 min		60 min
Concentration range	1 nM to 1 μ M	250 nM to 1 μ M	1 μ M	100 nM to 1 μ M	10 to 100 nM
Limit of detection	\sim 1 nM	0.19 μ M	—	—	10 nM
Resolution	50 pM	—	—	—	0.54 nM
Sensitivity	1 nm/ μ M	0.04 nm/ μ M	—	0.04 nm/nM	0.35 nm/nM 0.025 nm/nM
Regeneration	—	Yes	—	Yes	Yes

resonance peak position, which corresponds to the same wavelength shift obtained previously in different trials using only one step between TBA and 100 nM of thrombin. The absence of a wavelength shift from 50 to 100 nM suggests that the sensor reaches a saturation limit. Changes in the PLL/TBA concentrations in the functionalization procedure should give rise to improvement of the thrombin detection efficiency.

In the case of the LPFG, a smaller negative shift is observed. As previously mentioned, the wavelength shift attained for the same RI samples is 20 times higher than that for the SPR compared to the LPFG, as confirmed by the data. The lower sensitivity to the external RI shown by the LPFG was found to be a limitation to a proper quantification of the thrombin with accuracy. Nevertheless, it validated the working principle also with LPFG. Furthermore, several strategies can be explored to greatly enhance the sensitivity of LPFG-based devices³³ that could enable quantification.

Although the comparison between those two system devices can be achieved by the introduction of a figure of merit (FOM) by using the following equation:³⁴

$$\text{FOM} = \frac{S}{\text{FWHM}}, \quad (3)$$

which is defined by the ratio between the sensitivity to the external RI (S) and the full width at half maximum. Considering the sensitivities to the external medium previously calculated as 3143 nm/RIU and 204 nm/RIU for the SPR and LPFG sensors, respectively, the calculated FOM results in 26.2 and 18.3, which is an indicator of a better performance of the SPR configuration even with a wider spectral shape.

These results are comparable to other researchers' work, as can be observed in Table 1.

This comparison is made through the same recognition method using a DNA aptamer and it shows indicators of good performance considering the sensitivity to the thrombin detection and the total regeneration of the sensor surface.

3.4 Cross-Reactivity to Other Molecules

The TBA was already presented as an aptamer that shows good affinity and specificity against thrombin²⁶ and does not interact with other plasma proteins or thrombin analogues such as gamma-thrombin;²⁷ nevertheless, its cross-reactivity with other molecules was experimentally tested.

To assess the nonspecific binding of other molecules that could be present in real samples of the different sensor configurations, the LPFG and SPR sensing devices were incubated with 100 nM of human serum albumin (HSA) for 60 min in the same affinity buffer. Because HSA is the most abundant protein in human plasma and is a potential interference present in real blood or serum samples, it is a suitable protein to be tested in the present work.

In the case of the LPFG, the wavelength shift obtained has an insignificant value (\sim 0.022 nm), which was found to be below the measurement error. In the SPR configuration, a higher shift of about 0.9 nm was observed (data not shown), for 100 nM of HAS, however, this is a small fraction of the shift obtained when incubating with only 10 nM thrombin.

These results show good chemical and biological specificity of TBA binding to thrombin even in the presence of potential interferences.

4 Conclusions

The detection of thrombin was compared using two different optical fiber sensing configurations, LPFG- and SPR-based.

LPFG with titanium dioxide coating improves the sensitivity to external refractive indices and has proven the feasibility of thrombin detection. Despite the temperature dependence, the robustness and the narrow bands lead to possible applications with multiplexing capabilities. The coupling to FBGs allows the postprocessing corrections to thermal variations. The lower sensitivity to the external RI is a barrier to quantify the thrombin concentrations with accuracy. Nevertheless, it can be used to act for presence/absence detection.

The higher RI sensitivity of the SPR with a higher FOM when compared to the LPFG response and the insensitivity to thermal variations have shown detection levels of thrombin down to 10 nM. The regeneration of the surface was attained in both configurations allowing a new functionalization procedure and, therefore, the reuse of the sensing system.

Both refractometric platforms allow to use the external RI variations to quantify thrombin concentration in a buffer solution, therefore, the same concept could, in principle, be applied to estimate the RI/thickness of the PLL layer or even to quantify the amount of the TBA immobilization.

Acknowledgments

This work is financed by the North Portugal Regional Operational Programme (NORTE 2020), under the PORTUGAL

2020 Partnership Agreement, and through the European Regional Development Fund (ERDF) within projects POCI-01-0145-FEDER-006961 and Coral - Sustainable Ocean Exploitation: Tools and Sensors/NORTE-01-0145-FEDER-000036. L.C. acknowledges the support from FCT grant SFRH/BD/78149/2011.

References

- X.-D. Wang and O. S. Wolfbeis, "Fiber-optic chemical sensors and biosensors (2008-2012)," *Anal. Chem.* **85**(2), 487–508 (2013).
- I. R. Krauss et al., "Thrombin-aptamer recognition: a revealed ambiguity," *Nucleic Acids Res.* **39**(17), 7858–7867 (2011).
- A. Sosic et al., "Human thrombin detection through a sandwich aptamer microarray: interaction analysis in solution and in solid phase," *Sensors* **11**(10), 9426–9441 (2011).
- M. A. Shuman and P. W. Majerus, "The measurement of thrombin in clotting blood by radioimmunoassay," *J. Clin. Invest.* **58**(5), 1249–1258 (1976).
- A. D. Ellington and J. W. Szostak, "In vitro selection of RNA molecules that bind specific ligands," *Nature* **346**(6287), 818–822 (1990).
- S. Tombelli, M. Minunni, and M. Mascini, "Analytical applications of aptamers," *Biosens. Bioelectron.* **21**(12), 2424–2434 (2005).
- R. Stoltenburg, C. Reinemann, and B. Strehlitz, "SELEX—a (r) evolutionary method to generate high-affinity nucleic acid ligands," *Biomol. Eng.* **24**(4), 381–403 (2007).
- W. Mok and Y. Li, "Recent progress in nucleic acid aptamer-based biosensors and bioassays," *Sensors* **8**(11), 7050–7084 (2008).
- X. Li et al., "Electrochemical impedance spectroscopy for study of aptamer-thrombin interfacial interactions," *Biosens. Bioelectron.* **23**(11), 1624–1630 (2008).
- C. K. O'Sullivan, "Aptasensors—the future of biosensing?," *Anal. Bioanal. Chem.* **372**(1), 44–48 (2002).
- B. Deng et al., "Aptamer binding assays for proteins: the thrombin example—a review," *Anal. Chim. Acta* **837**, 1–15 (2014).
- R. Queirós et al., "Evanescent wave DNA-aptamer biosensor based on long period gratings for the specific recognition of E. coli outer membrane proteins," *Biosens. Bioelectron.* **62**, 227–233 (2014).
- J. Pollet et al., "Fiber optic SPR biosensing of DNA hybridization and DNA-protein interactions," *Biosens. Bioelectron.* **25**(4), 864–869 (2009).
- T. Allsop et al., "Aptamer-based surface plasmon fibre sensor for thrombin detection," *Proc. SPIE* **7715**, 77151C (2010).
- G. Rego, "A review of refractometric sensors based on long period fibre gratings," *Sci. World J.* **2013**, 913418 (2013).
- A. Vengsarkar et al., "Long-period fiber gratings as band-rejection filters," *J. Lightwave Technol.* **14**(1), 58–65 (1996).
- S. James and R. Tatam, "Optical fibre long-period grating sensors: characteristics and application," *Meas. Sci. Technol.* **14**(5), R49–R61 (2003).
- S. Korposh et al., "Fiber optic long period grating sensors with a nano-assembled mesoporous film of SiO₂ nanoparticles," *Opt. Express* **18**(12), 13227–13238 (2010).
- B. D. Gupta and R. K. Verma, "Surface plasmon resonance-based fiber optic sensors: principle, probe designs, and some applications," *J. Sens.* **2009**, 979761 (2009).
- J. Homola, S. S. Yee, and G. Gauglitz, "Surface plasmon resonance sensors: review," *Sens. Actuators, B* **54**(1–2), 3–15 (1999).
- G. Rego, J. Santos, and H. Salgado, "Refractive index measurement with long-period gratings arc-induced in pure-silica-core fibres," *Opt. Commun.* **259**(2), 598–602 (2006).
- O. Ivanov and G. Rego, "Origin of coupling to antisymmetric modes in arc-induced long-period fiber gratings," *Opt. Express* **15**(21), 13936–13941 (2007).
- L. Coelho et al., "Enhanced refractive index sensing characteristics of optical fibre long period grating coated with titanium dioxide thin films," *Sens. Actuators B* **202**, 929–934 (2014).
- K. O. Hill et al., "Bragg gratings fabricated in monomode photosensitive optical fiber by UV exposure through a phase mask," *Appl. Phys. Lett.* **62**(10), 1035–1037 (1993).
- L. Coelho et al., "Sensing structure based on surface plasmon resonance in chemically etched single mode optical fibres," *Plasmonics* **10**(2), 319–327 (2014).
- L. C. Bock et al., "Selection of single-stranded DNA molecules that bind and inhibit human thrombin," *Nature* **355**, 564–566 (1992).
- J. J. Li, X. Fang, and W. Tan, "Molecular aptamer beacons for real-time protein recognition," *Biochem. Biophys. Res. Commun.* **292**(1), 31–40 (2002).
- E. Fogg, A. N. Hixson, and A. R. Thompson, "Densities and refractive indexes for ethylene glycol-water solutions," *Anal. Chem.* **27**(10), 1609–1611 (1955).
- C. Berrettoni et al., "Fibre tip sensor with embedded FBG-LPG for temperature and refractive index determination by means of the simple measurement of the FBG characteristics," *J. Sens.* **2015**, 491391 (2015).
- L. Coelho et al., "Enhanced refractive index sensing characteristics of optical fibre long period grating coated with titanium dioxide thin films," *Sens. Actuators B-Chem.* **202**, 929–934 (2014).
- D. E. Gray, *American Institute of Physics Handbook*, McGraw-Hill, New York (1982).
- M. Westwood, T. R. Noel, and R. Parker, "The effect of poly-L-lysine structure on the pH response of polygalacturonic acid-based multilayers," *Carbohydr. Polym.* **94**(1), 137–146 (2013).
- A. Cusano et al., "Coated long-period fiber gratings as high-sensitivity photochemical sensors," *J. Lightwave Technol.* **24**(4), 1776 (2006).
- J.-T. Lin et al., "Analysis of scaling law and figure of merit of fiber-based biosensor," *J. Nanomater.* **2012**, 7 (2012).
- S.-F. Lin et al., "A guided mode resonance aptasensor for thrombin detection," *Sensors* **11**(9), 8953–8965 (2011).
- B.-J. Park et al., "Spectroscopic and electrochemical detection of thrombin/5'-SH or 3'-SH aptamer immobilized on (porous) gold substrates," *Bull. Korean Chem. Soc.* **33**(1), 100–104 (2012).
- L. Razquin et al., "Thrombin detection by means of an aptamer based sensitive coating fabricated onto LMR-based optical fiber refractometer," in *IEEE Sensors*, pp. 1–4, IEEE, Taipei (2012).

Luís Coelho received his graduate degree in physics engineering in 2005 and his MSc degree in instrumentation and microelectronics in 2007, both from the University of Coimbra, Portugal. In 2016, he received his PhD in physics at the University of Porto, Portugal, focusing on thin films technology applied to optical fiber sensors in collaboration with INESC TEC, Porto, Portugal. He is currently a postdoctoral researcher working in sensors for chemical and biochemical applications.

José Manuel Marques Martins de Almeida graduated in applied physics (optics and electronics) (1987) and has a PhD (1993) from the University of Porto, Portugal. Since 2000, he has had the position of associate professor at the Department of Physics, Universidade de Trás os Montes e Alto Douro, Portugal, and has habilitation (2006) from the same university. Currently, he is a senior researcher at the Centre for Applied Photonics at INESC TEC.

José Luís Santos graduated in applied physics (optics and electronics) from the University of Porto (1983), PhD (1993), and habilitation (2008) from the same university. His main research interests are related with optical fiber sensing and optical fiber technology. He holds the position of full professor of physics in the astronomy department of University of Porto and he is a researcher of INESC Porto Optoelectronics and Electronic Systems Unit. He is a member of OSA, SPIE, and the Planetary Society.

Pedro Alberto da Silva Jorge graduated in applied physics from the University of Minho (1996), MSc degree in optoelectronics and lasers from the University of Porto (2000), in 2006, he concluded his PhD at Porto University in collaboration with the University of Charlotte, North Carolina. He is a senior researcher at INESC TEC, where he leads the biochemical sensors team exploring the potential of optical fiber and integrated optics technologies, coordinating several projects in these areas.

Maria Cristina L. Martins is an expert in the development of biomaterial coatings. She received her PhD in engineering sciences at the Faculty of Engineering of the University of Porto in 2003 at Instituto de Engenharia Biomédica (INEB) and University of Washington

Engineered Biomaterials, Seattle, United States (UWEB). She has been an assistant investigator of INEB since 2005 and an affiliated professor at Instituto de Ciências Biomédicas Abel Salazar (ICBAS) of the University of Porto, Portugal.

Diana Viegas graduated in physics in 2003 and received her MSc degree in computational methods in science and engineering in 2006, both from the University of Porto, Portugal. She received her PhD for work microfabrication of optical devices for sensing applications at the University of Porto in 2010. She is performing some research in optical fiber sensors with surface plasmon resonance

field. Since 2014, she has been a research fellow at the International Iberian Nanotechnology Laboratory.

Raquel B. Queirós holds a diploma (2007) in chemical engineering and a master's degree (2008) in technologies for environmental protection both from Instituto Superior de Engenharia do Porto (ISEP). In 2013, she received her PhD in physics from the University of Porto, studying biosensors for the detection and quantification of bacterial contamination in water. She joined the International Iberian Nanotechnology Laboratory as a research fellow in 2014, where she is involved in detection of water biotoxins.